Generation and symmetry control of quantum frequency combs

G. Maltese, M. I Amanti, Félicien Appas, G. Sinnl, A Lemaitre, P. Milman, F. Baboux, S. Ducci

Generation and symmetry control of quantum frequency combs

G. Maltese,[1] M.I. Amanti*,[1] F. Appas,[1] G. Sinnl,[1] A. Lemaître,[2] P. Milman,[1] F.Baboux,[1] and S. Ducci[1]

[1] *Laboratoire Matériaux et Phénomènes Quantiques, Université Paris Diderot, CNRS-UMR 7162, Paris 75013, France*

[2] *Centre de Nanosciences et de Nanotechnologies, CNRS, Université Paris-Sud, Université Paris-Saclay, C2N-Marcoussis*

* Corresponding author

Email address: maria.amanti@univ-paris-diderot.fr

Quantum frequency combs are a useful resource for parallel quantum communication and processing, given the robustness and easy handling offered by the frequency degree of freedom. In this work we propose a method to generate broadband biphoton frequency combs and control their symmetry under particle exchange, based on purely passive optical components, such as a cavity and an optical delay line. We experimentally demonstrate our method using an integrated AlGaAs semiconductor platform producing quantum frequency combs, working at room temperature and compliant with electrical injection. We show the generation and manipulation of biphoton frequency combs, spreading over more the 500 peaks. These results open interesting perspectives for the development of massively parallel and reconfigurable systems for complex quantum operations.

INTRODUCTION

Since the emergence of the domain of quantum information, quantum optics plays an important role as an experimental test bench for a large variety of novel concepts; nowadays, in the framework of the development of quantum technologies, photonics represents a promising platform for several applications ranging from long distance quantum communications to the simulation of complex phenomena and metrology [1, 2]. In these last years a growing attention has been devoted to large scale entangled quantum states of light as key elements to increase the data capacity and robustness in quantum information protocols. Such states can be realized through qubits encoded in many-particles, but this approach suffers from scalability problems; an alternative strategy is to work with a lesser number of particles and to encode information in high-dimensional spaces. This has been implemented using different degrees of freedom of light: spatial or path modes [3, 4], orbital angular momentum [5, 6], time-energy [7], frequency [8, 9]. Among all these possibilities the frequency domain is particularly appealing thanks to its compatibility with the existing fibered telecom network [10]; moreover, it enables the development of robust and scalable systems in a single spatial mode, without the requirement of complex beam shaping or stabilized interferometers.

The most straightforward physical process to generate quantum states in the frequency domain is nonlinear optical conversion, widely used to produce photon pairs for quantum information and communications protocols.

A convenient way to handle the frequency continuous degree of freedom is to discretize it, generating biphoton frequency combs [11]. Such states have first been investigated exploiting spontaneous parametric down-conversion (SPDC) in dielectric crystals [12–14], by placing a resonant cavity either after or around the nonlinear material. In the latter case the state is shaped directly at the generation stage with the advantage of avoiding signal reduction [15]. More recently biphoton frequency combs have been generated in integrated optical micro-resonators via spontaneous four-wave mixing: this approach overcomes the drawbacks of low scalability and high cost of bulk systems. Interesting results on the generation and coherent manipulation of high-dimensional frequency states have been obtained in both Hydex [8] and silicon nitride micro-rings [9]. In this work, we propose a method to generate biphoton frequency combs and control their symmetry, by combining the spectral filtering effect of a cavity with the control of the temporal delay between photons of a pair. We demonstrate our method on an integrated AlGaAs semiconductor device emitting broadband frequency quantum states in the telecom range, working at room temperature and compliant with electrical injection [16]. The ability to switch from symmetric to anti-symmetric high-dimensional states opens the way to the implementation of qudits teleportation, logic gates as well as dense coding and state discrimination [6, 17, 18]. For instance as a generalization of well-known bipartite entanglement-assisted teleportation protocol, high dimensional antisymmetric frequency states are well suited for distributing quantum state between N parties. At the same time, the control over the symmetry of frequency combs can be exploited in multi-partite key-sharing communication protocols[19] as well as logic gate for encoding of robust qubits in high-dimensional redundant states [20].

We use an optical cavity to discretize the frequency joint spectral amplitude of a bi-photon state and a temporal delay between photons of a pair, to manipulate the quantum state. A shift in the time domain between the two photons of the quantum state corresponds, in the frequency domain, to a periodic symmetric and anti-symmetric modulation of the joint spectral amplitude, with periodicity fixed by the delay. For specific time shifts the choice of the pump frequency determines the symmetry under particle exchange of the quantum state. For photons delayed by odd multiples of the half of cavity round trip time, when the pump frequency is an even multiple of the cavity free spectral range, we generate a symmetric frequency comb, while for odd multiples the state is anti-symmetric. The tuning of the pump wavelength thus controls the spectral wavefunction and more specifically its symmetry. Optical cavities have already been used in SPDC quantum optics experiments to demonstrate the control over Hong-Ou-Mandel (HOM) interferometry: tuning of the cavity length drives the transition between photon coalescence and anti-coalescence [21–23]. However these schemes were not directly related to the framework of the quantum state manipulation and, with respect to our proposal, they rely on post-selection, as usual techniques based on coincidence measurements of photons emerging from a beam-splitter.

By contrast, we present here an experimental scheme to generate on demand symmetric and anti-symmetric biphoton frequency combs. Its implementation requires only purely passive optical components, such as a cavity and an optical delay line, leading to limited optical losses compared to recently demonstrated manipulation schemes based on active elements [8, 9], such as phase modulators. In addition, optical cavities and temporal delay lines are well suitable elements for an on-chip fully integrated quantum circuit.

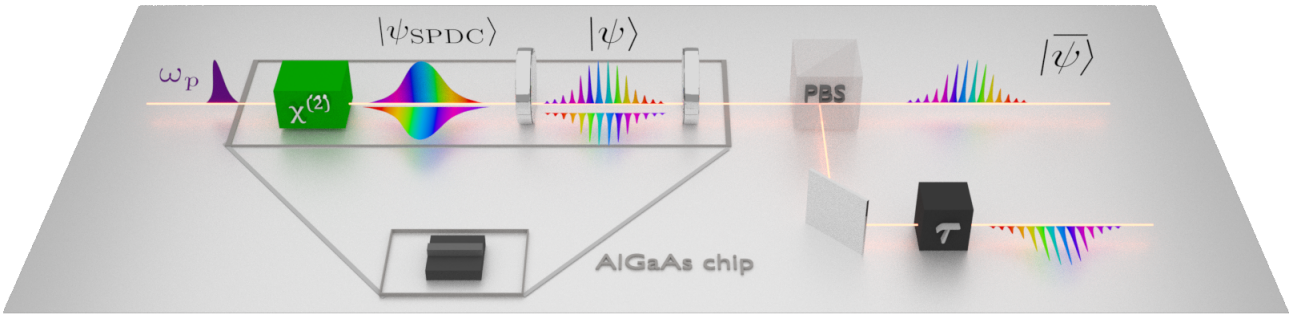

FIG. 1. Schematic of the experimental set-up for the generation and manipulation of biphoton frequency comb. Photons are represented by their spectrum. A monochromatic cw pump beam (ω_p) generates photon pairs in the state $|\psi_{SPDC}\rangle$ by type II SPDC. An optical cavity discretizes the spectrum of the emitted photons, producing a biphoton combs $|\psi\rangle$. The photons of each pair are deterministically separated with a polarizing beam splitter (PBS) and an optical delay τ is imposed between them, leading to the state $|\overline{\psi}\rangle$. The symmetry of $|\overline{\psi}\rangle$ is controlled by tuning the pump frequency ω_p.

RESULTS

Theory

In Figure 1 we present the schematic of the experimental set up for the generation and symmetry manipulation of biphoton frequency combs. Photon pairs are generated by type II SPDC in a nonlinear medium: a pump photon at the frequency ω_p annihilates, generating two orthogonally polarized photons called signal (at frequency ω_1) and idler (at frequency ω_2). The resulting quantum state can be written as:

$$|\psi_{SPDC}\rangle = \int_{-\infty}^{\infty}\int_{-\infty}^{\infty} C(\omega_1,\omega_2)\,|H,\omega_1\rangle\,|V,\omega_2\rangle\,d\omega_1 d\omega_2 \tag{1}$$

where $C(\omega_1,\omega_2)$ is the joint spectral amplitude (JSA), i.e. the amplitude probability density of generating one of the photons at frequency ω_1 with polarization H and the other at frequency ω_2 with polarization V. For convenience we write the state using the basis $\omega_+ = \omega_1 + \omega_2$ and $\omega_- = \omega_1 - \omega_2$; in this case, the JSA function takes the expression $C(\omega_+,\omega_-) = C_p(\omega_+)C_{PM}(\omega_+,\omega_-)$, where C_p is the pump spectral profile and C_{PM} is the phase matching function related to the material properties. If we consider the pump frequency range where the generated photons have degenerate frequencies, the non-linear conversion has its maximum efficiency and C_{PM} is in good approximation a symmetric function in ω_-, centered in $\omega_- = 0$, whose bandwidth depends on the characteristics of the nonlinear medium [24]. An optical cavity discretizes the frequency space of the state $|\psi_{SPDC}\rangle$ (See Figure 1). At this stage the function C_{cav} associated to the cavity, which is the product of the signal and idler cavity transmission functions ($C_{cav} = T_s(\omega_1)T_i(\omega_2) = C_{cav}(\omega_+,\omega_-)$), modulates the state JSA. The resulting state is a biphoton frequency comb, consisting in a sequence of phase-locked evenly-spaced peaks with a common phase originating from the pump [12]. Figure 2 (a) presents the numerical simulation of the corresponding joint spectral intensity (JSI=$|(C_p(\omega_+)C_{PM}(\omega_+,\omega_-)C_{cav}(\omega_+,\omega_-)|^2$), which represents the experimental measurement of the state frequency spectrum, relaxing the requirement of phase sensitive techniques [8, 25, 26] ~~which is the accessible function for experimental measurements~~. We show a zoom of the JSI around $\omega_- = 0$, for a cavity consisting of a Fabry-Perot resonator of mirror reflectivity R=0.8, free spectral range $\bar{\omega}$ and a pump laser of bandwidth $\Delta\omega \gg \bar{\omega}$. We observe that the JSI presents a periodic pattern with a fixed periodicity $2\bar{\omega}$ in both ω_+ and ω_- directions. The number of peaks in the ω_+ direction is determined by the width of the pump spectral profile, while the one in the ω_- direction is determined by the width of the C_{PM} function.

In the case of a monochromatic pump beam (linewidth $\Delta\omega \ll \bar{\omega}$), the pump spectral profile can be approximated as $C_p(\omega_+) = \delta(\omega_+ - \omega_p)$. The corresponding quantum state at the output of the cavity is:

$$|\psi\rangle = \int_{-\infty}^{\infty} C_{PM}(\omega_p, \omega_-) C_{cav}(\omega_p, \omega_-) d\omega_- \\ |H, \frac{\omega_p + \omega_-}{2}\rangle |V, \frac{\omega_p - \omega_-}{2}\rangle \tag{2}$$

By tuning of the pump frequency we have access to two classes of states, having different spectral patterns (See Figure 2(a) dashed lines). For $\omega_p = \omega_R = 2n\bar{\omega}$ (resonant frequency), with n integer number, we generate resonant states $|\psi_R\rangle$, whose JSI maxima are disposed at even multiple of $\bar{\omega}$ (See Figure 2(b)). In the approximation of a cavity with very high reflectivity, the resonant state is:

$$|\psi_R\rangle = \sum_m \int_{-\infty}^{\infty} C_{PM}(\omega_R, \omega_- - 2m\bar{\omega}) d\omega_- \\ |H, \frac{\omega_R + \omega_-}{2}\rangle |V, \frac{\omega_R - \omega_-}{2}\rangle \tag{3}$$

where m is an integer number, spanning the frequency peaks of the photon pairs. For $\omega_p = \omega_{AR} = (2n+1)\bar{\omega}$ (anti-resonant frequency), we generate anti-resonant states $|\psi_{AR}\rangle$, whose JSI maxima are disposed at odd multiples of $\bar{\omega}$ (See Figure 2(c)). In the same approximation of a cavity with perfect reflectivity the anti-resonant state is:

$$|\psi_{AR}\rangle = \sum_m \int_{-\infty}^{\infty} -C_{PM}(\omega_{AR}, \omega_- - (2m+1)\bar{\omega}) d\omega_- \\ |H, \frac{\omega_{AR} + \omega_-}{2}\rangle |V, \frac{\omega_{AR} - \omega_-}{2}\rangle \tag{4}$$

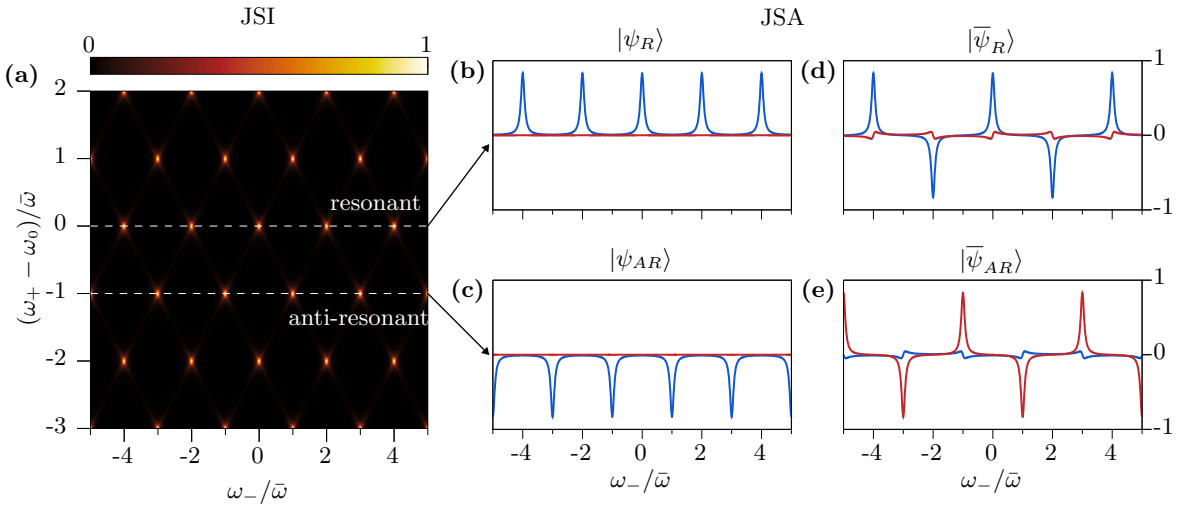

FIG. 2. a) Simulated JSI of the quantum state generated through type II SPDC filtered by a Fabry Perot resonator with mirror reflectivity 0.8, for a pump beam of linewidth $\Delta\omega \gg \bar{\omega}$ and central frequency ω_0, coinciding with the cavity resonance closest to degeneracy. Dashed lines evidence two cuts of the JSI corresponding to a resonant and an anti-resonant state.
(b-c) Corresponding simulation of the JSA (blue line: real part (symmetric); red line: imaginary part (anti-symmetric)), for $\tau = 0$ (d, e) and $\tau = \pi/\bar{\omega}$ (d, e).

The simulated JSA for intermediate values of the pump beam frequency is presented in the Supplementary Information (See Figure 1-2 Supplementary Information).

In order to control the symmetry of the biphoton state, we introduce a third stage in the experimental setup, consisting of a polarizing beam splitter, separating deterministically the signal and idler photons into two different paths a and b, and a delay line on one of the two paths (see Figure 1). The introduced temporal delay τ modulates the JSA of the state $|\psi\rangle$ with the periodic function $f_{delay} = \exp(i\tau\omega_-)/2 = \cos(\tau\omega_-)/2 + i\sin(\tau\omega_-)/2$, consisting of a symmetric real part and anti-symmetric imaginary part in the ω_- variable. For $\tau = \pi/\bar{\omega}$, corresponding to half of the cavity round trip time, the periodicity f_{delay} is the double of the one of $|\psi\rangle$ state's JSA. In this case, the JSA of

the resonant state $|\psi_R\rangle$ is in phase with the symmetric part of f_{delay}, resulting in the pattern of Figure 2(d). On the contrary the JSA of the anti-resonant state $|\psi_{AR}\rangle$ is in phase with the anti-symmetric part of f_{delay} resulting in the pattern of Figure 2(e). The resonant and anti-resonant states after the optical delay stage are:

$$\begin{aligned} |\overline{\psi}_R\rangle &= \sum_m C_{PM}(\omega_R, 2m\bar{\omega}) e^{im\pi} \\ &\qquad |a, \frac{\omega_R}{2} + m\bar{\omega}\rangle\, |b, \frac{\omega_R}{2} - m\bar{\omega}\rangle \\ |\overline{\psi}_{AR}\rangle &= \sum_m C_{PM}(\omega_{AR}, (2m+1)\bar{\omega}) e^{i(m+1)\pi} \\ &\qquad |a, \frac{\omega_{AR}}{2} + (m+\frac{1}{2})\bar{\omega}\rangle\, |b, \frac{\omega_{AR}}{2} - (m+\frac{1}{2})\bar{\omega}\rangle \end{aligned} \tag{5}$$

We note that the state $|\overline{\psi}_R\rangle$ is symmetric under particles exchange, while $|\overline{\psi}_{AR}\rangle$ is anti-symmetric. Analog results occur for τ values that are odd multiples of the cavity half round-trip time (see Figure 3 in Supplementary Information). We have thus demonstrated that the proposed experimental setup enables the generation of symmetric and anti-symmetric biphoton frequency combs by tuning of the pump laser frequency.

Experiments

In the following, we experimentally demonstrate this method using an AlGaAs chip (See Methods). This platform combines a large second order optical susceptibility, a direct bandgap and a high electro-optic effect, making it attractive for the miniaturization and the integration of several quantum fonctionalities in a single chip [27, 28]. Figure 3 reports the experimental measurement of the joint spectral intensity JSI=$|C(\omega_+, \omega_-)|^2$ of the quantum state at the output of the AlGaAs chip, measured over a frequency range of 10 $\bar{\omega}$ (Numerical simulations are reported in Supplementary Figure 2). The measurement is done by stimulated emission tomography [25] for two values of the pump beam frequency separated by $\bar{\omega}$. We observe spectra having a periodic pattern due to the Fabry Perot cavity effect of the AlGaAs chip waveguide. Peaks are centered at even or odd multiples of the free spectral range ($\bar{\omega}$), depending on the pump frequency. These results prove that the device emits a biphoton frequency comb and that the tuning of the pump frequency controls the transition from a resonant state to an anti-resonant one. We notice that even if the facet reflectivity of AlGaAs chip is lower than 0.3 (See Methods), since C_{cav} is the product of $T_s(\omega_1)T_i(\omega_2)$, we demonstrate a significant modulation of the frequency state. In order to quantify the level of mirror symmetry of

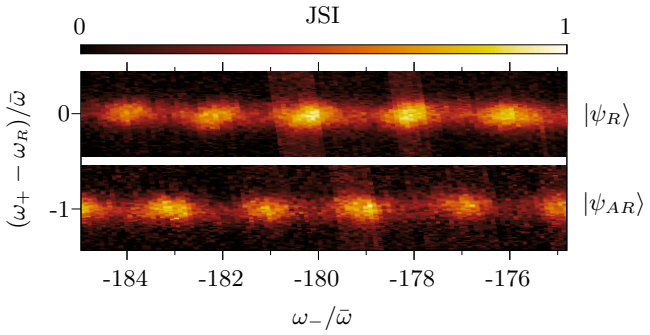

FIG. 3. JSI of the state generated by the AlGaAs chip measured by stimulated emission tomography for two values of the pump beam frequency, ω_p=ω_R and ω_p=$\omega_R - \bar{\omega}$ corresponding to a resonant and an anti-resonant state, respectively. $\bar{\omega} = 2\pi \cdot 19.2$ GHz, $\omega_R = 2\pi \cdot 392.120$ THz (764.313 nm)

the JSA function, we implement a HOM interferometer (See Methods). In Figure 4 we report the result for $|\psi_R\rangle$: a dip having a width of 52 ±2 fs is observed. Similar results are expected for $|\psi_{AR}\rangle$ (See Figure 6 of Supplementary Information). The dip visibility defined as $|N_\tau - N_0|/N_\tau$, where N_τ is the coincidences rate far from the interference region and N_0 the coincidence rate at zero delay, is 86%. This value is limited by a residual modal birefringence reducing photon indistinguishability. The oscillating behavior observed around the dip is well described by taking into account the chromatic dispersion of the sample, as shown by the result of the numerical simulation reported in Figure 4, based on the nominal AlGaAs structure. From this simulation we can extract the emission bandwidth of

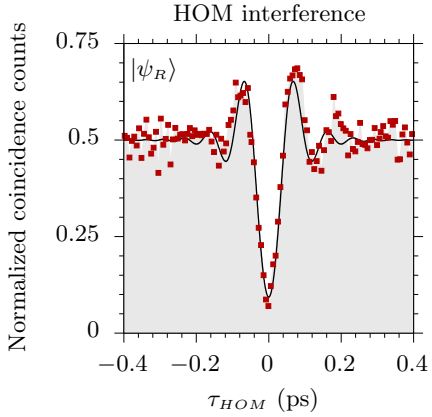

FIG. 4. Results of the HOM measurement of the state $|\psi_R\rangle$ produced at the output of the AlGaAs chip. Squares: experimental data. Line: theoretical model.The obtained visibility is 0.86 and the spectral bandwidth of the interfering photons is 170 nm.

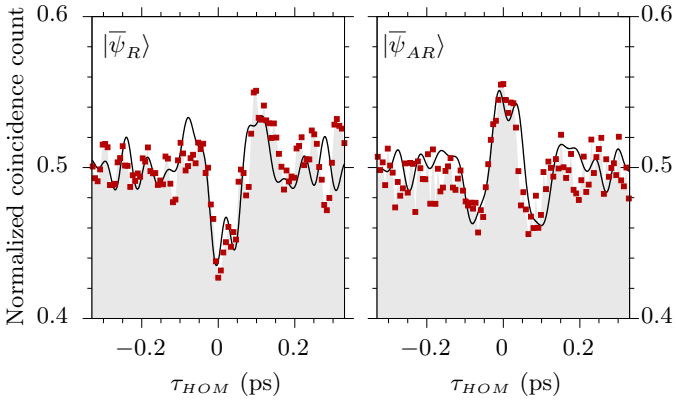

FIG. 5. Results of the HOM measurement of the (left) resonant state $|\overline{\psi}_R\rangle$ and (right) anti-resonant state $|\overline{\psi}_{AR}\rangle$. Line: theoretical model.

the photon pairs, $\Delta\omega_- = 2\pi \cdot 21.82$ THz, corresponding to a signal and idler bandwidth of $\Delta\lambda_{s,i} = 170.9$ nm around 1530 nm (see details in Supplementary Information Figure 4-5). This result demonstrates that the device generates a broadband biphoton frequency comb, where the photons of each pair are in a superposition of more than 500 peaks.

To implement the proposed manipulation scheme we separate the photons of each pair by a polarizing beam splitter and we introduce a delay line set to $\tau = \pi/\bar{\omega}$, as presented in Figure 1 (See Methods). Tuning the pump frequency at resonance (antiresonance) condition, we generate the state $|\overline{\psi}_R\rangle$ ($|\overline{\psi}_{AR}\rangle$) at the output of the delay line.

In order to evaluate the symmetry of the JSA of these states, we rely again on HOM interferometry: photon pairs described by a symmetric JSA are expected to bunch, whereas photon pairs described by an anti-symmetric wave function are expected to anti-bunch [29].As photons are bosons, the global wavefunction describing their state is indeed symmetric. If the symmetry of the spectral part of the biphoton state is modified, its spatial component changes accordingly, in order to preserve the overall state symmetry. Figure 5 reports the experimental results of the HOM experiment for the state $|\overline{\psi}_R\rangle$ (left panel) and the state $|\overline{\psi}_{AR}\rangle$ (right panel). For resonant $|\overline{\psi}_R\rangle$/anti-resonant $|\overline{\psi}_{AR}\rangle$ state we report a dip/peak of $\approx 10\%$ visibility around zero delay. This result proves that the tuning of the pump frequency manipulates the spectrum of quantum frequency combs, changing the weight of symmetric and anti-symmetric components of the state. The measured visibility is limited by the combined effect of cavity reflectivity, birefringence and chromatic dispersion. Indeed in the case of low reflectivity the transmission function of the cavity has resonances with limited visibility and as a consequence it shapes only a restrained part of the state. In addition, as for results in Figure 4, residual birefringence and chromatic dispersion limit photons indistinguishability. The experimental results are interpreted by a numerical model of our system based on the nominal AlGaAs structure: starting from the quantum state simulated from the measurements presented in Figure 4, we include the cavity and delay effect. In Figure 5 we report the results of this numerical simulation and we demonstrate a very good agreement with experiments.

DISCUSSION

In conclusion, we have proposed and demonstrated a method to generate and manipulate the symmetry of biphoton frequency combs based on the interplay between cavity effects and temporal delay between photons of a pair. The method can be adapted and applied to a large variety of systems, either bulk or integrated, thus increasing their flexibility and the richness of the generated states. Moreover since it does not rely on post selection, it can generate on demand anti-symmetric states. We have shown that AlGaAs Bragg reflector waveguides are a particularly convenient system to implement this method, thanks to the emission of photon pairs via type II SPDC (leading to a deterministic separation of the photon pairs), small birefringence of the generated modes (leading to a symmetric JSA with respect to frequency degeneracy and avoiding the requirement of off-chip compensation), and to the natural presence of a cavity (due to facets reflectivity). We predict by numerical simulation that, given the characteristics of the AlGaAs chip, a spectral filter centered at the frequency degeneracy and having a bandwidth of 25 nm, together with a reflection coating increasing the facets reflectivity to 0.5, would allow to reach a visibility of 70% for $|\overline{\psi}_R\rangle$ and $|\overline{\psi}_{AR}\rangle$ states. We discuss the estimated visibility in the ideal case of zero birefringence (or compensated birefringence) and zero chromatic dispersion as a function of the reflectivity in the Supplementary Information Figure 6. Further progress is possible in different ways: a full integration of the setup could be obtained by developing an on-chip polarizing beam splitter, as already demonstrated in Si-based devices [30],Si on insulator[31], Lithium Niobate[32], and high performance solution have been proposed using machine learning based devices [33]. In addition the fine tuning of the relative delay between the orthogonally polarized photons can be implemented through the electro-optic effect [34]. Moreover, the compliance of AlGaAs chips with electrical injection at room temperature [16] paves the way towards the integration of the laser source within the chip, resulting in an extremely miniaturized and versatile system. We note that in contrast to approaches based on the manipulation of each resonance mode with active components such as phase modulators [8, 9], our scheme directly manipulates the comb as a whole, by relying only on passive elements well suited for on-chip integration. This simple and robust scheme can be exploited for novel applications in quantum information, such as the production of single qubit gates and error correction in a measurement-based architecture [20], opening the way to further applications and scaling in quantum computing. In addition, the free spectral range of our devices is around 20 GHz, smaller than that of state-of-the-art microring resonators [8, 9], leading to a larger spectral density of resonances. The states produced by our source thus have a strong potential in terms of high-density encoding, yet, within our approach the resources needed for the manipulation of such high-dimensional states is independent on the size of the state, making this approach well suited for large-scale applications. Overall, these results open the way to new quantum protocols exploiting high-dimensional frequency states with controllable symmetry, such as the implementation of quantum logic gates through coherent manipulation of entangled frequency-bin qubits [35], high-dimensional one-way quantum processing [36] or error correction in high-dimensional redundant states [20].

METHODS

AlGaAs chip. AlGaAs chip consists of a Bragg reflection ridge waveguide optimized for efficient type II SPDC [16, 37, 38]. It consists of a 6-period $Al_{0.80}Ga_{0.20}/Al_{0.25}Ga_{0.75}As$ Bragg reflector (lower mirror), a 298 nm $Al_{0.45}Ga_{0.55}As$ core, and a 6-period $Al_{0.25}Ga_{0.75}As$ / $Al_{0.80}Ga_{0.20}$ Bragg reflector (upper mirror). Waveguides are fabricated using wet chemical etching to define $\sim$10 μm wide and $\sim$5 μm deep ridges along the (011) crystalline axis, in order to exploit the maximum nonzero optical nonlinear coefficient and a natural cleavage plane. The modes involved in the nonlinear process are a TE Bragg mode for the pump beam around 765 nm and TE_{00} and TM_{00} modes for the photon pairs in the C-telecom band. Note that, for this device, the group velocity mismatch between the two photons of each pair is so small that no off-chip compensation is required to preserve their indistinguishably to a high level [28, 39]. The photon pairs are thus emitted in very good approximation with a joint spectral amplitude centered in $\omega_- = 0$ and symmetric in the ω_- variable, enabling a direct implementation of our method. Experimental measurements of the coincidence rate and coincidence to accidental ratio (CAR) of typical AlGaAs device are reported in Supplementary Figure 8. For an input power of 15 μW and a 2 mm long device, we report the detection of 90 Hz and a CAR of around 3200. Moreover, the refractive index contrast between the semiconductor and the air, leads to a modal reflectivity at the waveguide facets of 0.27(0.24) for the TE(TM) polarized mode, creating a Fabry-Perot cavity surrounding the nonlinear medium with a finesse of about 2.

Experimental set-up. A schematic of the experimental set-up is presented in supplementary Figure 7. Photon pairs are generated by pumping the device with a CW diode laser (TOPTICA TM Photonics DL pro 780), providing a tunable quasi- monochromatic pump beam within the frequency range of ω_p= [2473, 2340] THz($\lambda_p = [762, 805]nm$),

with a linewidth $\Delta\nu_p \approx 100$kHz. The free spectral range of the cavity ($\bar{\omega} = 2\pi \cdot 19.2$ GHz) is much larger than the pump laser linewidth. A small fraction of the pump beam is sent to an Optical Spectrum Analyzer (OSA, Yokogawa TM AQ6370C) to monitor its wavelength. The main fraction of the beam is sent through an in-house made holographic mask (HM). The mask grating is designed to convert an incoming Gaussian beam into a waveguide Bragg eigenmode. A polarizer (P) sets the polarization of the pump beam to the horizontal direction (H-polarized or TE). A half-wave plate (HWP) is placed before the polarizer to finely control the pump power. The pump laser is coupled into the waveguide through a microscope objective having a high numerical aperture (NA=0.95, 63X). Typical input power at the objective if of 20 mW. In this regime multiple-pairs generation have been neglected.. A thermocouple and a Peltier cooler, connected to a PID controller, monitor and keep the waveguide temperature constant at 20 °C. The output coupling is done via a second microscope objective (NA=0.65, 40X) and the pump power measured at this stage is of few tens of μ W. A frequency low-pass filter blocks the transmitted pump beam, while the photon pairs are coupled in the fibered part of the setup through a fibered coupler (FC). The photons of each pair are separated by a polarizing beam splitter (PBS). A polarization controller (PC) is used to align the photons polarization axis with the ones of the PBS. In order to perform HOM interferometry at the output of the polarizing beam splitter, an additional fiber PC compensates the ellipticity acquired by the two photons during their propagation along the fibers and sets parallel polarization in the two arms of the interferometer. The difference in optical lengths between these two arms is controlled by a free space delay line, which consists in a fixed fiber coupler (FC) and a FC mounted on a motorized stage (ThorLabs TM MTS50/M-Z8). At the beam-splitter output photons are sent to two single-photon detectors (Free-running InGaAs/InP avalanche photodiodes, idQuantique TM ID230). Each detector efficiency is set to 25% and dead time to 25μs. A time-to-digital converter (TDC, QuTau TM QuTools) measures the time differences between the detection events of each detector in a start and stop configuration.

DATA AVAILABILITY

The data and analysis codes used in this study are available from the corresponding author on request.

ACKNOWLEDGEMENT

The authors gratefully acknowledge ANR (Agence Nationale de la Recherche) for the financial support of this work through Project SemiQuantRoom (Project No. ANR-14-CE26-0029) and through Labex SEAM (Science and Engineering for Advanced Materials and devices) project ANR 11 LABX 086, ANR 11 IDEX 05 02.The French RENATECH network and Université Sorbonne Paris Cité for PhD fellowship to G.M. are also warmly acknowledged.

ADDITIONAL INFORMATION

Competing interests: The authors declare no competing interests.

AUTHOR CONTRIBUTIONS

G.M. Conceived and designed the experiments and fabricated the samples. G.M with the contribution of M.A, G.S and F.A performed the experiments. G.M carried out data analysis and theoretical work with the guidance of M.A and critical input of P.M, F.B and S.D. M.A. , G.M and S.D wrote the paper with the contribution of of all the authors. A.L. performed epitaxial growth of the AlGaAs sample. M.A and SD supervised the project and the work.

[1] F. Flamini, N. Spagnolo, and F. Sciarrino, Reports on Progress in Physics **82**, 016001 (2018).
[2] V. Giovannetti, S. Lloyd, and L. Maccone, Nature photonics **5**, 222 (2011).
[3] M. N. O'Sullivan-Hale, I. Ali Khan, R. W. Boyd, and J. C. Howell, Phys. Rev. Lett. **94**, 220501 (2005).
[4] M. Krenn, R. Fickler, M. Huber, R. Lapkiewicz, W. Plick, S. Ramelow, and A. Zeilinger, Phys. Rev. A **87**, 012326 (2013).
[5] M. McLaren, M. Agnew, J. Leach, F. S. Roux, M. J. Padgett, R. W. Boyd, and A. Forbes, Opt. Express **20**, 23589 (2012).
[6] Y. Zhang, F. S. Roux, T. Konrad, M. Agnew, J. Leach, and A. Forbes, Science advances **2**, e1501165 (2016).

[7] R. T. Thew, A. Acín, H. Zbinden, and N. Gisin, Phys. Rev. Lett. **93**, 010503 (2004).
[8] M. Kues, C. Reimer, P. Roztocki, L. R. Corts, S. Sciara, B. Wetzel, Y. Zhang, A. Cino, S. T. Chu, B. E. Little, D. J. Moss, L. Caspani, J. Azaa, and R. A. A. Morandotti, Nature **546**, 622 (2017).
[9] P. Imany, J. A. Jaramillo-Villegas, O. D. Odele, K. Han, D. E. Leaird, J. M. Lukens, P. Lougovski, M. Qi, and A. M. Weiner, Opt. Express **26**, 1825 (2018).
[10] L. Olislager, J. Cussey, A. T. Nguyen, P. Emplit, S. Massar, J.-M. Merolla, and K. P. Huy, Phys. Rev. A **82**, 013804 (2010).
[11] M. Kues, C. Reimer, J. M. Lukens, W. J. Munro, A. M. Weiner, D. J. Moss, and R. Morandotti, Nature Photonics **13**, 170 (2019).
[12] Y. J. Lu, R. L. Campbell, and Z. Y. Ou, Phys. Rev. Lett. **91**, 163602 (2003).
[13] Z. Xie, T. Zhong, S. Shrestha, X. Xu, J. Liang, Y.-X. Gong, J. C. Bienfang, A. Restelli, J. H. Shapiro, F. N. C. Wong, and C. A. Wei Wong, Nature Photonics **9**, 536 (2015).
[14] R.-B. Jin, R. Shimizu, M. Fujiwara, M. Takeoka, R. Wakabayashi, T. Yamashita, S. Miki, H. Terai, T. Gerrits, and M. Sasaki, Quantum Science and Technology **1**, 015004 (2016).
[15] Y. Jeronimo-Moreno, S. Rodriguez-Benavides, and A. B. U'Ren, Laser Physics **20**, 1221 (2010).
[16] F. Boitier, A. Orieux, C. Autebert, A. Lemaître, E. Galopin, C. Manquest, C. Sirtori, I. Favero, G. Leo, and S. Ducci, Phys. Rev. Lett. **112**, 183901 (2014).
[17] S. K. Goyal, P. E. Boukama-Dzoussi, S. Ghosh, F. S. Roux, and T. Konrad, Scientific Reports **4**, 4543 EP (2014), article.
[18] I. Jex, G. Alber, S. Barnett, and A. Delgado, Fortschritte der Physik **51**, 172 (2003).
[19] I. Jex, G. Alber, S. Barnett, and A. Delgado, Fortschritte der Physik **51**, 172 (2003), https://onlinelibrary.wiley.com/doi/pdf/10.1002/prop.200310021.
[20] N. Fabre, G. Maltese, F. Appas, S. Felicetti, A. Ketterer, A. Keller, T. Coudreau, F. Baboux, M. Amanti, S. Ducci, and P. Milman, "Continuous variables error correction with integrated biphoton frequency combs," (2019), arXiv:1904.01351 [quant-ph].
[21] M. A. Sagioro, C. Olindo, C. H. Monken, and S. Pádua, Phys. Rev. A **69**, 053817 (2004).
[22] C. Olindo, M. Sagioro, C. Monken, S. Pádua, and A. Delgado, Physical Review A **73**, 043806 (2006).
[23] A. Zavatta, S. Viciani, and M. Bellini, Phys. Rev. A **70**, 023806 (2004).
[24] M. Barbieri, E. Roccia, L. Mancino, M. Sbroscia, I. Gianani, and F. Sciarrino, Scientific reports **7**, 7247 (2017).
[25] A. Eckstein, G. Boucher, A. Lematre, P. Filloux, I. Favero, G. Leo, J. E. Sipe, M. Liscidini, and S. Ducci, Laser & Photonics Reviews **8**, L76 (2014).
[26] I. Jizan, B. Bell, L. G. Helt, A. C. Bedoya, C. Xiong, and B. J. Eggleton, Opt. Lett. **41**, 4803 (2016).
[27] A. Orieux, M. A. M. Versteegh, K. D. Jns, and S. Ducci, Reports on Progress in Physics **80**, 076001 (2017).
[28] T. Günthner, B. Pressl, K. Laiho, J. Geßler, S. Höfling, M. Kamp, C. Schneider, and G. Weihs, Journal of Optics **17**, 125201 (2015).
[29] A. Fedrizzi, T. Herbst, M. Aspelmeyer, M. Barbieri, T. Jennewein, and A. Zeilinger, New Journal of Physics **11**, 103052 (2009).
[30] H. Cai, C. M. Long, C. T. DeRose, N. Boynton, J. Urayama, R. Camacho, A. Pomerene, A. L. Starbuck, D. C. Trotter, P. S. Davids, et al., Optics Express **25**, 12282 (2017).
[31] H. Xu, D. Dai, and Y. Shi, Laser & Photonics Reviews **13**, 1970021 (2019), https://onlinelibrary.wiley.com/doi/pdf/10.1002/lpor.201970021.
[32] H.-P. Chung, C.-H. Lee, K.-H. Huang, S.-L. Yang, K. Wang, A. S. Solntsev, A. A. Sukhorukov, F. Setzpfandt, and Y.-H. Chen, Opt. Express **27**, 1632 (2019).
[33] E. Lucas, G. Lihachev, R. Bouchand, N. G. Pavlov, A. S. Raja, M. Karpov, M. L. Gorodetsky, and T. J. Kippenberg, Nature Photonics **12**, 699 (2018).
[34] J. Wang, A. Santamato, P. Jiang, D. Bonneau, E. Engin, J. W. Silverstone, M. Lermer, J. Beetz, M. Kamp, S. Höfling, et al., Optics Communications **327**, 49 (2014).
[35] J. A. Jaramillo-Villegas, P. Imany, O. D. Odele, D. E. Leaird, Z.-Y. Ou, M. Qi, and A. M. Weiner, Optica **4**, 655 (2017).
[36] C. Reimer, S. Sciara, P. Roztocki, M. Islam, L. Romero Cortés, Y. Zhang, B. Fischer, S. Loranger, R. Kashyap, A. Cino, S. T. Chu, B. E. Little, D. J. Moss, L. Caspani, W. J. Munro, J. Azaña, M. Kues, and R. Morandotti, Nature Physics **15**, 148 (2019).
[37] P. Yeh and A. Yariv, Optics Communications **19**, 427 (1976).
[38] A. Helmy, Optics express **14**, 1243 (2006).
[39] C. Autebert, N. Bruno, A. Martin, A. Lemaitre, C. G. Carbonell, I. Favero, G. Leo, H. Zbinden, and S. Ducci, Optica **3**, 143 (2016).